

## Simulation of a collisionless planar electrostatic shock in a proton–electron plasma with a strong initial thermal pressure change

This article has been downloaded from IOPscience. Please scroll down to see the full text article.

2010 Plasma Phys. Control. Fusion 52 025001

(<http://iopscience.iop.org/0741-3335/52/2/025001>)

[The Table of Contents](#) and [more related content](#) is available

Download details:

IP Address: 143.117.13.152

The article was downloaded on 19/01/2010 at 10:11

Please note that [terms and conditions apply](#).

# Simulation of a collisionless planar electrostatic shock in a proton–electron plasma with a strong initial thermal pressure change

M E Dieckmann<sup>1,2,3</sup>, G Sarri<sup>1</sup>, L Romagnani<sup>1</sup>, I Kourakis<sup>1</sup> and M Borghesi<sup>1</sup>

<sup>1</sup> Centre for Plasma Physics, Queen's University Belfast, Belfast BT7 1NN, UK

<sup>2</sup> Theoretische Physik IV, Ruhr-University Bochum, 44780 Bochum, Germany

<sup>3</sup> Department of Science and Technology (ITN), Linköping University, Campus Norrköping, 60174 Norrköping, Sweden

E-mail: [Mark.E.Dieckmann@itn.liu.se](mailto:Mark.E.Dieckmann@itn.liu.se)


Received 24 June 2009, in final form 25 October 2009

Published 18 January 2010

Online at [stacks.iop.org/PPCF/52/025001](http://stacks.iop.org/PPCF/52/025001)

## Abstract

The localized deposition of the energy of a laser pulse, as it ablates a solid target, introduces high thermal pressure gradients in the plasma. The thermal expansion of this laser-heated plasma into the ambient medium (ionized residual gas) triggers the formation of non-linear structures in the collisionless plasma. Here an electron–proton plasma is modelled with a particle-in-cell simulation to reproduce aspects of this plasma expansion. A jump is introduced in the thermal pressure of the plasma, across which the otherwise spatially uniform temperature and density change by a factor of 100. The electrons from the hot plasma expand into the cold one and the charge imbalance drags a beam of cold electrons into the hot plasma. This double layer reduces the electron temperature gradient. The presence of the low-pressure plasma modifies the proton dynamics compared with the plasma expansion into a vacuum. The jump in the thermal pressure develops into a primary shock. The fast protons, which move from the hot into the cold plasma in the form of a beam, give rise to the formation of phase space holes in the electron and proton distributions. The proton phase space holes develop into a secondary shock that thermalizes the beam.

 This article features multimedia enhancements

(Some figures in this article are in colour only in the electronic version)

## 1. Introduction

The impact of a laser pulse on a solid target results in the evaporation of the target material. The heated plasma expands under its own thermal pressure and shocks as well as other non-linear plasma structures form. Generating collisionless plasma shocks in a laboratory experiment permits us to study their detailed dynamics in a controlled manner. A better understanding of such shocks is relevant not only for the laser-plasma experiment as such but also for inertial confinement fusion experiments. It can also provide further insight into the dynamics of solar system shocks and the non-relativistic astrophysical shocks, such as the supernova remnant shocks [1–5].

An obstacle to an in-depth investigation of the laser-generated shocks has been, so far, that the frequently used optical probing techniques could not resolve the shock structure at the required spatio-temporal resolution. The now available proton imaging technique [6, 7] helps us to overcome this limitation. This method can provide accurate spatial electric field profiles at a high time resolution, as long as no strong magnetic fields are present. The non-relativistic flow speed of the laser-generated shock, e.g. that in [8], implies that no strong self-induced magnetic fields due to the filamentation instability or the mixed mode instability [9, 10] occur at the shock front.

The availability of electric field data at a high resolution serves as a motivation to perform related numerical simulations and to compare their results with the experimental ones. The experimental observations from [8], which are most relevant for the simulation study we perform here, can be summarized as follows. The ablation of a solid target consisting of aluminium or tungsten by a laser pulse with a duration of  $\approx 470$  ps and an intensity of  $10^{15}$  W cm $^{-2}$  results in a plasma with a density of  $\approx 10^{18}$  cm $^{-3}$  and with an electron temperature of a few kiloelectronvolts. This plasma expands into an ambient plasma with the density of  $\leq 10^{15}$  cm $^{-3}$ . The ambient plasma has been produced mainly by a photo-ionization of the residual gas. The dominant components of the residual gas, which consists of diluted air, are oxygen and nitrogen. Electrostatic structures, which move through the ionized residual gas, are observed. Their propagation speeds suggest that one is an electrostatic shock [11] with a thickness of a few electron Debye lengths, which expands approximately with the ion acoustic velocity of  $2\text{--}4 \times 10^5$  m s $^{-1}$ . Ion-acoustic solitons trail the shock. Another structure moves at twice the shock speed, which is probably related to a shock-reflected ion beam. The electron–electron, electron–ion and ion–ion mean-free paths for the residual gas have been determined for this particular experiment. They are of the order of centimetres and much larger than the shock width of a few tens of micrometres. The shock and the electrostatic structures are collisionless.

The experiment can measure the electric fields, the propagation speed of the electric field structures and it can estimate the electron temperature and density. The bulk parameters of the ions, such as their temperature, mean speed and ionization state, are currently inaccessible, as well as detailed information about the spatial distribution of the plasma. We can set up a plasma simulation with the experimentally known parameters, and we can introduce an idealized model for the unknown initial conditions. The detailed information about the state of the plasma, which is provided by Vlasov simulations [12] or by particle-in-cell (PIC) simulations [13, 14], can then provide further insight into the expansion of this plasma.

Here we investigate a mechanism that could result in the shock observed in [8]. We model with PIC simulations the interplay of two plasmas with a large difference in the thermal pressure, which are initially spatially separated. We aim to determine the spatio-temporal scale, over which a shock forms under this initial assumption, and we want to reveal the structures that develop in the wake of the shock. The temperature and density of the hot laser-ablated

plasma both exceed initially that of the cold ambient plasma by two orders of magnitude. The density ratio is less than that between the expanding and the ambient plasma in [8]. However, the density will not change in the form of a single jump in the experiment and realistic density changes will probably be less or equal to the one we employ. Selecting the same jump in the density and temperature is computationally efficient, because both plasmas have the same Debye length that determines the grid cell size and the allowed time step. The ion temperature in the experiment is likely to be less than that of the electrons. The electron distribution can also not be approximated by two separate spatially uniform and thermal electron clouds, because the plasma generation is not fast compared with the electron diffusion. We show, however, that the shock forms long after the electrons have diffused in the simulation box and reached almost the same temperature everywhere.

A change in the thermal pressure by a factor of  $10^4$  should imply a plasma expansion that is similar to that into a vacuum. This process has received attention in the context of auroral, astrophysical and laser-generated plasmas and it has been investigated analytically within the framework of fluid models [15, 16] or Vlasov models [17, 18]. It has been modelled numerically using a cold ion fluid and Boltzmann-distributed electrons [19] and with kinetic Vlasov and PIC simulations [20, 21]. The plasma expansion of hot electrons and cold ions into a tenuous medium has also been examined with PIC simulations, such as the pioneering study in [22], which reported the formation of a double layer [23–25] that cannot form if the plasma expands into a vacuum. Our simulation also examines the dynamics of protons as a first step towards the simulation of a mixture of oxygen and nitrogen ions that constitute the residual gas in the physical experiment. Notable differences between the expansion of the hot and dense plasma into the ambient plasma and the expansion into a vacuum are observed.

The structure of this paper is as follows. We describe the PIC method in section 2 and give the initial conditions and the simulation parameters. Section 3 models the initial phase of the plasma expansion at a high phase space resolution, revealing details of the electron expansion and of the quasi-equilibrium, which is established for the electrons. A double layer develops at the thermal pressure jump, which drags the electrons from the tenuous plasma into the hot plasma in the form of a cold beam. The electrons from the hot plasma leak into the cold plasma, which reduces the temperature difference between both plasmas. Section 4 examines the proton dynamics. The ambient plasma modifies the proton expansion. The thermal pressure jump evolves into a shock, which moves approximately with the proton thermal speed of the hot plasma. If the plasma expands into a vacuum, then a plasma density change can only be accomplished by ion beams [21], while the plasma is here compressed by the shock. The fastest protons in our simulation form a beam that outruns the shock. It interacts with the protons of the ambient medium to form phase space holes in the electron and proton distributions. The proton phase space holes develop into a secondary shock ahead of the primary one. This process may result in secondary shocks in experiments, similar to the radiation-driven ones [26]. The results are summarized in section 5.

## 2. The PIC simulation method and the initial conditions

A PIC code approximates a plasma by an ensemble of computational particles (CPs), each of which represents a phase space volume element. Each CP follows a phase space trajectory that is determined through the Lorentz force equation by the electric field  $\mathbf{E}(\mathbf{x}, t)$  and the magnetic field  $\mathbf{B}(\mathbf{x}, t)$ . Both fields are evolved self-consistently in time using Maxwell's equations and the macroscopic current  $\mathbf{J}(\mathbf{x}, t)$ , which is the sum over the microcurrents of all CPs. The standard PIC method considers only collective interactions between particles, although some collisional effects are introduced through the interaction of CPs with the field fluctuations [27].

Collision operators have been prescribed for PIC simulations [28, 29]. The structures in the addressed experiment form and evolve into a plasma, in which collisional effects are not strong and such operators are thus not introduced here. We may illustrate this with the help of the electron collision rate  $\nu_e \approx 2.9 \times 10^{-6} n_e \ln \Lambda T_e^{-3/2} \text{ s}^{-1}$  and the ion collision rate  $\nu_i \approx 4.8 \times 10^{-8} Z^4 \mu^{-1/2} n_i \ln \Lambda T_i^{-3/2} \text{ s}^{-1}$  [30] for a spatially uniform plasma with the number density  $n_e = n_i = 10^{15} \text{ cm}^{-3}$  and the temperature  $T_e = T_i = 10^3 \text{ eV}$ . We take a Coulomb logarithm  $\ln \Lambda = 10$  and we consider oxygen with  $\mu = 16$ . Both collision rates are comparable, if the mean ion charge  $Z \approx 4$ . We assume  $\nu_e \approx \nu_i$ . The electron plasma frequency  $\omega_p \approx 10^{12} \text{ s}^{-1}$  gives the low relative collision frequency  $\nu_e/\omega_p \approx 10^{-6}$ . The plasma flow in the experiment and other aspects, which are not taken into account by this simplistic estimate, alter this collision frequency. The mean-free path has been estimated to be of the order of a centimetre [8] and the ion beam with the speed  $4 \times 10^5 \text{ m s}^{-1}$  crosses this distance during the time  $\omega_p t \approx 25\,000$ . This presumably forms the upper time limit, for which we can neglect collisions.

The presence of particles with kiloelectronvolt energies and the preferential expansion direction of the plasma in the experiment imply that multi-dimensional PIC simulations should be electromagnetic in order to resolve the potentially important magnetic Weibel instabilities, which are driven by thermal anisotropies [31]. Such instabilities can grow in the absence of relativistic beams of charged particles, but they are typically weaker than the beam-driven ones [32]. Here we restrict our simulation to one spatial dimension  $x$  (1D) and we set  $B(x, t = 0)$ . The plasma expands along  $x$  and all particle beams will have velocity vectors aligned with  $x$ . The magnetic beam-driven instabilities have wavevectors that are oriented obliquely or perpendicular to the beam velocity vector and they are not resolved by a 1D simulation. The wavevectors, which are destabilized by the Weibel instability, can be aligned with the simulation direction, but only if the plasma is cooler along  $x$  than orthogonally to it. Such a thermal anisotropy can probably not form. Our electromagnetic simulation confirms that no magnetic instability grows. The ratio of the magnetic to the total energy remains at noise levels below  $10^{-4}$ .

A 1D PIC simulation should provide a reasonable approximation to those sections of the expanding plasma front observed in [8], which are planar over a sufficiently wide spatial interval orthogonal to the expansion direction. We set the length of the 1D simulation box as  $L$ . Plasma 1 consists of electrons (species 1) and protons (species 2), each with the density  $n_h$  and the temperature  $T_h = 1 \text{ keV}$ , and it fills up the half-space  $-L/2 < x < 0$ . A number density  $n_h = 10^{15} \text{ cm}^{-3}$  should be appropriate with regard to the experiment. The half-space  $0 < x < L/2$  is occupied by plasma 2, which is composed of electrons (species 3) and protons (species 4) with the temperature  $T_c = 10 \text{ eV}$  and the density  $n_c = n_h/100$ . All plasma species have initially a Maxwellian velocity distribution, which is at rest in the simulation frame.

The ablated target material drives the plasma expansion but its ions are probably not involved in the evolution of the shock and of the other plasma structures. These structures are observed already 100–200 ps after the laser impact at a distance of about 1 mm from the target. Aluminium ions, which are with a mass  $m_A$ , the lightest constituents of the target material, would have the thermal speed  $(T/m_A)^{1/2} \approx 10^5 \text{ m s}^{-1}$  for  $T = 1 \text{ keV}$ . Hundred times this speed or a temperature of 10 MeV would be necessary for them to propagate 1 mm in 0.1 ns. We thus assume here that the shock and the other plasma structures involve only the ions of the residual gas, which is air at a low pressure. If we assume that these ions have a high ionization state and comparable charge-to-mass ratios, then the protons may provide a reasonable approximation to their dynamics.

The equations solved by the PIC code are normalized with the number density  $n_h$ , the plasma frequency  $\Omega_1 = (n_h e^2 / m_e \epsilon_0)^{1/2}$  and the Debye length  $\lambda_D = v_{t1} / \Omega_1$  of species 1, which equals that of the other species. The thermal speeds of the respective species are  $v_{tj} = (T_j / m_j)^{1/2}$ , where  $j$  is the species index. We express the charge  $q_k$  and mass  $m_k$  of the  $k$ th CP in units of the elementary charge  $e$  and electron mass  $m_e$ . Quantities in physical units have the subscript p and we substitute  $\mathbf{E}_p = \Omega_1 v_{t1} m_e \mathbf{E} / e$ ,  $\mathbf{B}_p = \Omega_1 m_e \mathbf{B} / e$ ,  $\mathbf{J}_p = e v_{t1} n_h \mathbf{J}$ ,  $\rho_p = e n_h \rho$ ,  $x_p = \lambda_D x$ ,  $t_p = t / \Omega_1$ ,  $\mathbf{v}_p = \mathbf{v} v_{t1}$  and  $\mathbf{p}_p = m_e m_k v_{t1} \mathbf{p}$ . The 1D PIC code solves with  $\tilde{v}_{t1} = v_{t1} / c$  the equations

$$\nabla \times \mathbf{B} = \tilde{v}_{t1}^2 (\partial_t \mathbf{E} + \mathbf{J}), \quad \nabla \times \mathbf{E} = -\partial_t \mathbf{B}, \quad \nabla \cdot \mathbf{E} = \rho, \quad \nabla \cdot \mathbf{B} = 0, \quad (1)$$

$$\partial_t \mathbf{p}_k = q_k (\mathbf{E}[x_k] + \mathbf{v}_k \times \mathbf{B}[x_k]), \quad d_t x_k = v_{k,x}. \quad (2)$$

The Lorentz force is solved for each CP with index  $k$ , position  $x_k$  and velocity  $\mathbf{v}_k$ . It is necessary to interpolate the electromagnetic fields from the grid to the particle position to update  $\mathbf{p}_k$  and the microcurrents of each CP have to be interpolated to the grid to update the electromagnetic fields. Interpolation schemes are detailed in [13]. Our code is based on the virtual particle electromagnetic particle-mesh method [14] and it uses the lowest possible interpolation order possible with this scheme. Our code is parallelized through the distribution of the CPs over all processors.

Simulation 1 (section 3) resolves the box length  $L_S = 3350$  by  $N_S = 5 \times 10^3$  grid cells of size  $\Delta_{xS} = 0.67 \lambda_D$ . The dense species 1 and 2 are each resolved by  $8 \times 10^4$  CPs per cell and the tenuous species 3 and 4 by 800 CPs per cell, respectively. The simulation is evolved in time for the duration  $t_S = 800$ , subdivided into 45 000 time steps  $\Delta t_S$ . Simulation 2 in section 4 resolves the box length  $L_L = 10 L_S$  by  $N_L = 2.5 \times 10^4$  grid cells of size  $\Delta_{xL} = 1.34 \lambda_D$ . This grid cell size is sufficiently small to avoid a significant numerical self-heating [33] of the plasma during the simulation time. The total energy in the simulation is preserved to within  $\approx 10^{-5}$ . Species 1 and 2 are approximated by 6400 CPs per cell each and species 3 and 4 by 64 CPs per cell, respectively. The system is evolved during  $t_L = 25500$  with  $6.4 \times 10^5$  time steps.

We use periodic boundary conditions for the particles and the fields in all the directions. Ideally, no particles or waves should traverse the full box length during the simulation duration. The group velocity for the electrostatic waves and the propagation speed of the electrons are both comparable to  $v_{t1}$ . We obtain  $v_{t1} t_S / L_S \approx 0.24$  for simulation 1 and  $v_{t1} t_L / L_L \approx 0.76$  for simulation 2. Both simulations ran on 16 CPUs on an AMD Opteron cluster (2.2 GHz). Simulation 1/2 ran for 100/800 h.

### 3. Simulation 1: initial development

Our initial conditions involve a jump in the bulk plasma properties at  $x \approx 0$ . Some electrons of plasma 1 will expand into the half-space  $x > 0$  occupied by plasma 2. The slow protons cannot keep up with the electrons and the resulting charge imbalance gives rise to an electrostatic field  $E_x$ . This  $E_x$  confines the electrons of plasma 1 and it accelerates the electrons from plasma 2 into the half-space  $x < 0$ . The electrons of plasmas 1 and 2 with  $x < 0$  are separated along the velocity direction by the electrostatic potential and form a double layer.

Figure 1 examines the  $E_x$  and its potential. The amplitude of  $E_x$  peaks initially at  $x \approx 0$  and it accelerates the electrons into the negative  $x$ -direction. The position of the maximum of  $E_x$  moves to larger  $x$  with increasing times and the peak amplitude decreases. The spatial profile of  $E_x$  is smooth, which contrasts the one that drives the plasma expansion into a vacuum that has a cusp [21]. The potential difference of  $\approx 5$  kV between plasmas 1 and 2 remains unchanged. The spatial interval, in which the amplitude of  $E_x$  is well above noise

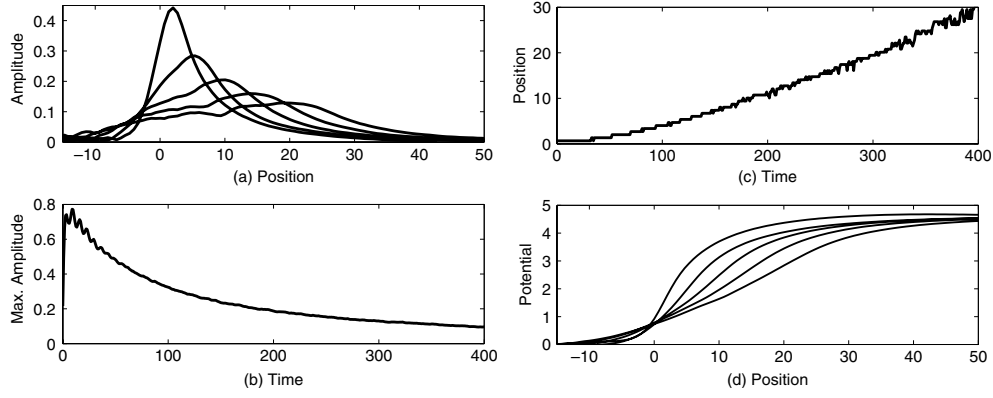


**Figure 1.** The electric field: (a) shows  $E_x$  at the times  $t = 60, 120, 180, 240$  and  $300$ . The maximum amplitude decreases with time as (b) shows and the location of the electric field maximum moves towards positive  $x$  (c). The potential in kilovolts obtained from the  $E_x$  distributions from (a) is displayed in (d). The potential jump remains unchanged, but the gradient is eroded with time.

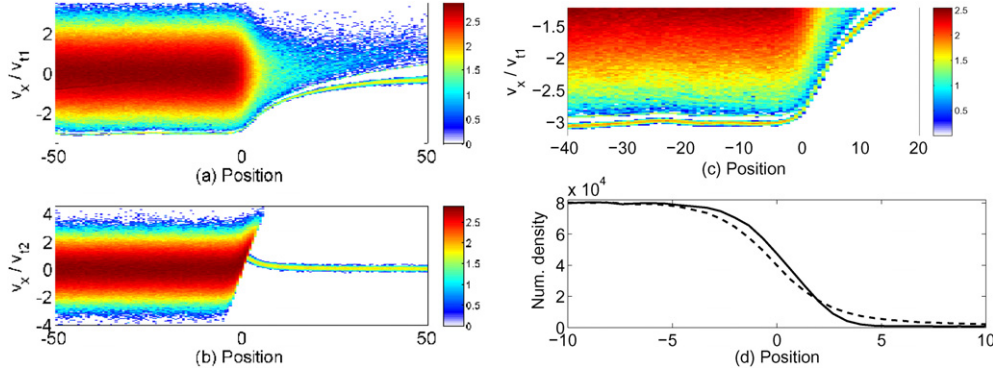


**Figure 2.** The plasma distribution at  $t = 60$ : (a) shows the electron phase space distribution. Most electrons from the dense plasma remain confined to  $x < 0$ , but some diffuse into the tenuous plasma. (b) shows the proton phase space distribution. Some protons with  $v_x > 0$  are accelerated in  $0 < x < 5$ . The protons with  $x, v_x < 0$  stream freely to lower values of  $x$ . (c) The electron phase space distribution reveals a double layer. (a)–(c) show the 10-logarithmic number of CPs. (d) shows the number of CPs per cell of the electrons (dashed curve) and the protons (solid curve). (Colour online.)

levels, is bounded. An interesting property of the double layer can thus be inferred according to [25]. Its electrostatic field can only redistribute the momentum between the four plasma species, but it cannot provide a net flow momentum. This is true if the double layer is one-dimensional and electrostatic. The decrease in the peak electric field in figure 1(b) resembles that in figure 3 in [19]. The decreasing electric force, in turn, implies that the ion acceleration in figure 4 of [19] decreases as time progresses, which should hold for our simulation too.

The plasma phase space distribution at  $t = 60$  is investigated in figure 2. A tenuous hot beam of electrons diffuses from plasma 1 into the half-space  $x > 0$ , while the mean speed of the electrons of plasma 2 becomes negative. The electrons of plasmas 1 and 2 with  $x < 0$  are separated by a velocity gap of  $\approx v_{t1}/10$ . The protons that were close to the initial boundary

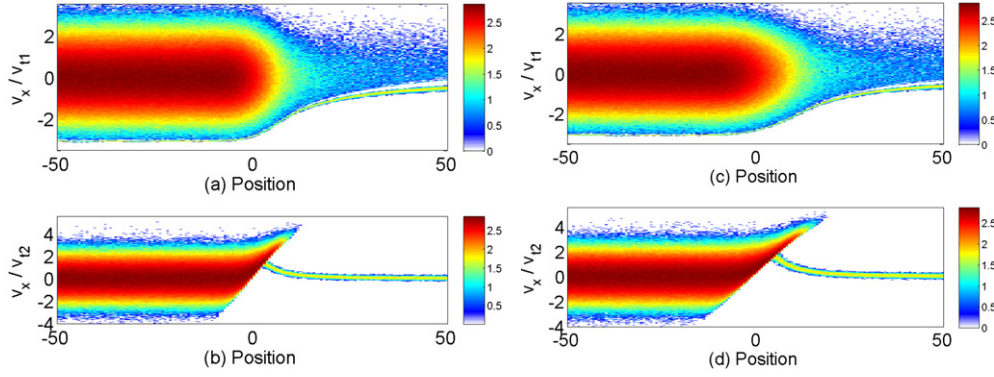


**Figure 3.** The 10-logarithmic phase space densities in units of CPs: the electron distribution in (a) and the proton distribution in (b) are sampled at  $t = 120$ , while (c) and (d) show them at  $t = 180$ . The protons in the interval  $x, v_x < 0$  convect almost freely away from  $x = 0$ . The protons of the dense plasma in  $x, v_x > 0$  accelerate. Electrons diffuse from plasma 1 into plasma 2 and form a hot beam, while electrons from plasma 2 enter plasma 1 in the form of a cold beam. (Colour online.)

$x = 0$  at  $t = 0$  have propagated until  $t = 60$  for a distance, which is proportional to their speed. A sheared velocity distribution can thus be seen in figure 2(b). The fastest protons of plasma 1 with  $x > 0$  have also been accelerated by the  $E_x$  by about  $v_{t2}/2$ , reaching now a peak speed of  $\approx 4v_{t2}$ . The fastest protons are found to the right of the maximum of  $E_x$  at  $x \approx 2$  at  $t = 60$  in figure 1(a). A similar acceleration is observed for the protons of plasma 2 in  $0 < x < 5$ . The densities of the electrons and protons disagree in the interval  $-5 < x < 5$  and the net charge results in the electrostatic field  $E_x > 0$ . Both curves in figure 2(d) intersect at  $x \approx 2$ , which coincides with the position in figure 1(a), where the  $E_x$  has its maximum at  $t = 60$ .

The density of the cold protons in [21] is practically discontinuous at the front of the expanding plasma, while it changes smoothly in our simulation. This is a result of our high proton temperature, which causes the thermal diffusion of the protons. The contour lines of the electron phase space density are curved at  $x \approx 0$ . Most electrons of plasma 1 that move to increasing values of  $x$  are reflected by the electrostatic potential at  $x \approx 0$ . These density contour lines resemble those of the distribution of electrons that expand into a vacuum at an early time in [21], which are all reflected by the potential at the plasma front. Here the inflow of electrons from plasma 2 into plasma 1 allows some of the electrons of plasma 1 to overcome the potential. The electrons provide all the energy for the proton expansion in [21] and their distribution develops a flat top. Here the proton thermal energy is the main driver and consequently the electron velocity distribution shows no clear deviation from a Maxwellian at any time.

Figure 3 shows the plasma phase space distributions at the times  $t = 120$  and  $t = 180$ . The plasma distributions are qualitatively similar to that in figure 2. The electrons diffuse out from plasma 1 into plasma 2, forming a hot beam, while the electrons of plasma 2 are dragged into the half-space  $x < 0$  in the form of a cold beam. The confined electrons of plasma 1 expand to increasing  $x$  at a speed, which is determined mainly by the protons. The proton distribution shows an increasing velocity shear, but the apparent phase space boundary between the protons of plasma 1 and 2 still intersects  $v_x = 0$  at  $x = 0$ . The front of the protons of plasma 1 at  $t = 120$  and  $t = 180$  is close to the position of the maximum of  $E_x$  in figure 1(a) at  $x \approx 5$  for  $t = 120$  and  $x \approx 10$  for  $t = 180$ . The protons at the front of plasma 1



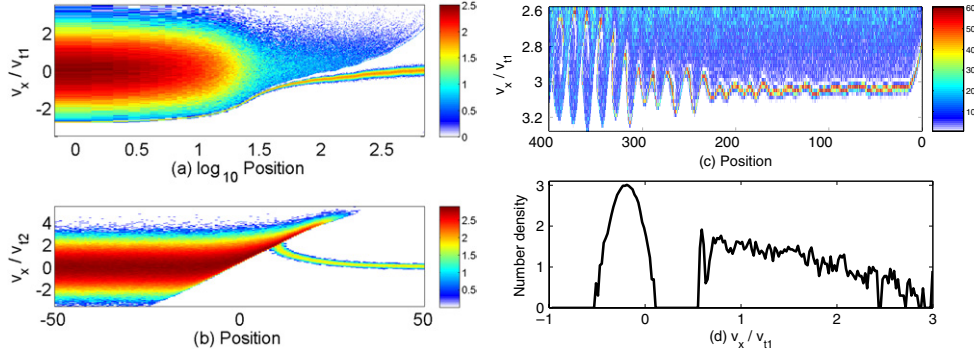


**Figure 4.** The 10-logarithmic number of CPs representing the electrons (a) and the protons (b) at the time  $t = 300$ . The electrons of plasma 1 have spread out to  $x \approx 700$ . The protons of plasma 1 with  $x > 0$  are accelerated to about  $5v_{t2}$ . The electron density in units of CPs for  $x < 0$  is displayed in (c). Electron phase space holes are present for  $x < -300$ . The electron distribution integrated over  $250 < x < 260$  is shown in (d). (Colour online.)

and the protons of plasma 2 in the same interval are accelerated by the  $E_x > 0$  and reach the peak speed  $\approx 5v_{t2}$ .

The electrons of plasma 1 in figure 4 at  $t = 300$  have expanded into the half-space  $x > 0$  for several hundred Debye lengths. The electrons from plasma 2, which have been dragged towards  $x < 0$ , interact with the electrons of plasma 1 through a two-stream instability. A chain of large electron phase space holes has developed for  $-400 < x < -300$ , which thermalize the beam distribution. No two-stream instability is yet observed in the interval  $x > 0$ , even though a beam distribution is present, for example at  $x \approx 250$ . The change in the mean speed of the electron beam leaked from plasma 1 for  $x > 0$  inhibits the resonance that gives rise to the two-stream instability. The mean speed of the electrons of plasma 2 does not vanish any more and it varies along  $x > 0$  to provide the return current that cancels that of the electrons of plasma 1. The  $E_x$  has noticeably accelerated the protons in the interval  $10 < x < 30$ , which still show the sheared distribution in the interval  $-25 < x < 25$ .

The evolution of the plasma is animated in movies 1 ([stacks.iop.org/PPCF/52/025001](http://stacks.iop.org/PPCF/52/025001)) (electrons) and 2 ([stacks.iop.org/PPCF/52/025001](http://stacks.iop.org/PPCF/52/025001)) (protons). The axis labels  $v_{eh} = v_{t1}$  and  $v_{ph} = v_{t2}$ . The colour scale denotes the 10-logarithmic number of CPs. Movie 1 reveals that a thin band of electrons parallel to  $v_x$  propagates away instantly from plasma 1 and towards  $x > 0$ . These electrons leave plasma 1, before the  $E_x$  has grown. The electrons diffusing into  $x > 0$  at later times, when the  $E_x$  has developed, form a tenuous beam with a broad velocity spread. The electrons of plasma 1 can overcome the double layer potential of  $\approx 5$  kV if their speed is  $v \geq 3v_{t1}$  prior to the encounter of its electrostatic field. Movie 1 furthermore illustrates the growth of the two-stream instability between the electron beam originating from plasma 2 and the confined electrons of plasma 1 in  $x < 0$  and its saturation through the formation of electron phase space holes. Movie 2 demonstrates how the velocity shear of the protons develops and how the fastest protons of plasma 1 in  $x > 0$  are accelerated by  $E_x$ . Neither figure 4 nor movie 2 reveals the formation of a shocked proton distribution prior to the time  $t_S$ .

We expand the simulation box and we reduce the statistical representation of the plasma. Ideally, the plasma evolution should be unchanged. Figure 5 compares the plasma data provided by simulation 1 (box length  $L_S$ ) and by simulation 2 ( $L_L = 10L_S$ ) at the time  $t_S$ , when we stop simulation 1. The proton distributions in both simulations are practically identical and we notice only one quantitative difference. The sheared proton distribution of plasma 1 extends

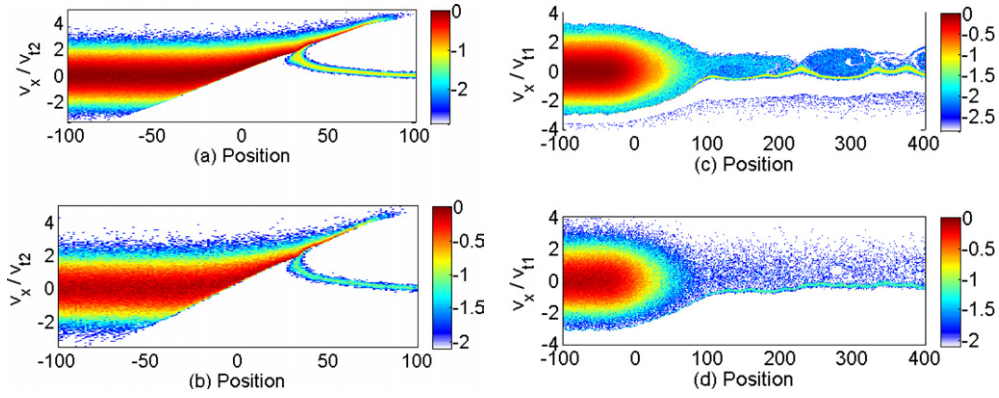


**Figure 5.** The 10-logarithmic phase space distributions, normalized to their respective peak values: (a) shows the proton distribution in simulation 1 and (b) that in simulation 2. The electron distributions in simulations 1 and 2 are displayed in (c) and (d), respectively. (Colour online.)

to  $x \approx -60$  and  $v_x \approx -3v_{t2}$  in simulation 1, while it reaches only  $x \approx -50$  and  $v_x \approx -2v_{t2}$  in simulation 2. This can be attributed to the better representation of the high-energy tail of the Maxwellian in simulation 1.

The bulk electron distributions in both simulations agree well for  $x < 100$ . The interaction of the confined electrons of plasma 1 with the expanding protons is thus reproduced well by both simulations. We find a beam of electrons with  $x > 100$  and  $v_x \approx -3v_{t1}$  in figure 5(c), which is accelerated by the double layer to  $-4v_{t1}$  in the interval  $-100 < x < 100$ . This beam originates from the second boundary between the dense and the tenuous plasma at  $x = L_S/2$  in simulation 1. It is thus an artefact of our periodic boundary conditions. Its density is three orders of magnitude below the maximum one and it thus does not carry significant energy. This tenuous beam does not show any phase space structuring, which would be a consequence of instabilities, and it has thus not interacted with the bulk plasma. Its only consequence is to provide a weak current that should not modify the double layer. This fast beam is absent in figure 5(d), because the electrons could not cross the distance  $L_L/2$  in simulation 2 during the time  $t_S$ .

The electron distributions for  $x > 100$  and  $v_x > 0$  computed by both simulations differ substantially. The electrons form phase space vortices in simulation 1, while the electrons in simulation 2 form a diffuse beam with some phase space structures, e.g. at  $x \approx 300$ . Phase space vortices are a consequence of an electrostatic two-stream instability, which must have developed between the leaked electrons of plasma 1 and the electrons of plasma 2. Only the electrons of plasma 1 with  $v > 3v_{t1}$  can overcome the double layer potential. These leaked electrons form a smooth beam in simulation 1 that can interact resonantly with the electrons of plasma 2 to form well-defined phase space vortices. The statistical representation of the leaking electrons in simulation 2 provides a minimum density that exceeds the density of these vortices.

#### 4. Simulation 2: Long term evolution

We examine the plasma at three times. The snapshot  $S_1$  corresponds to the time  $t = 8000$ ,  $S_2$  to  $t = 16000$  and  $S_3$  to  $t = 25500$ . The plasma phase space distributions for  $S_1$  and  $S_2$  are displayed in figure 6. The proton distribution is still qualitatively similar to that at  $t = 300$  in

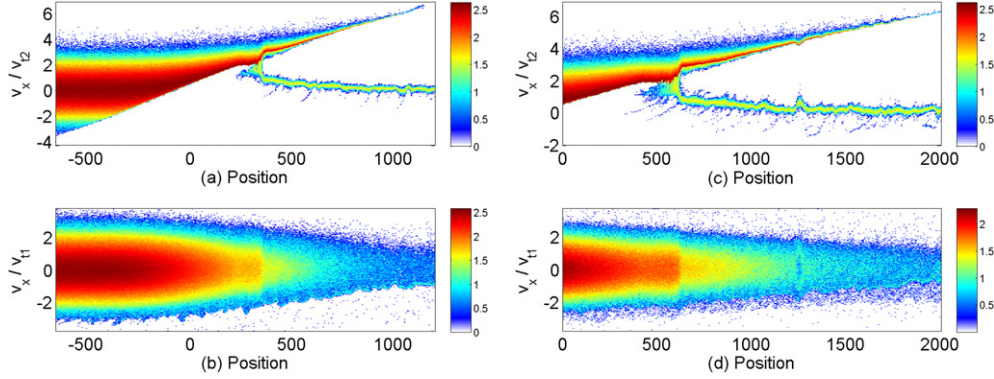


**Figure 6.** The 10-logarithmic phase space distributions of the snapshots  $S_1$  (a), (b) and  $S_2$  (c), (d) in units of CPs: a shock develops in the proton distribution (a) at  $x \approx 300$ . The electrons are distributed symmetrically around  $v_x = 0$  in (b) and their density value jumps at  $x \approx 300$ . The proton shock in (c) and the electron density jump in (d) have propagated to  $x \approx 600$  at the mean speed  $\approx v_{t2}$ . (Colour online.)

figure 4. The phase space boundary between the protons of plasmas 1 and 2 has been tilted further by proton streaming. The key difference between figures 4 and 6 is found, where the proton distribution of plasma 1 merges with that of plasma 2. This collision boundary is located at  $x \approx 300$  for  $S_1$  and at  $x \approx 600$  for  $S_2$ , which evidences an approximately constant speed of this intersection point. The propagation speed is  $\approx v_{t2}$ . The protons directly behind this collision boundary, e.g. in  $450 < x < 550$  for  $S_2$ , do not show a velocity shear. Their mean speed and velocity spread is spatially uniform in this interval, evidencing the downstream region of a shock. The upstream proton distribution with  $x > 600$  for  $S_2$  resembles, however, only qualitatively that of an electrostatic shock [11]. That consists of the incoming plasma and the shock-reflected ion beam. The density of the beam with  $v_x \approx 4v_{t2}$  exceeds that of plasma 2 in the same interval and its mean speed exceeds  $v_s \approx v_{t2}$  of the shock by a factor 4. A shock-reflected ion beam would move at twice the shock speed and its density would typically be less than that of the upstream plasma, which the shock reflects. The linear increase in the proton beam velocity with increasing  $x$  is reminiscent of the plasma expansion into a vacuum [20], but here it is a consequence of the shear introduced by the proton thermal spread.

The electron distribution at  $t = t_S$  in figure 5(d) could be subdivided into the cold electrons of plasma 2 and the leaked hot electrons of plasma 1, while the electrons in the interval  $x > 750$  have a symmetric velocity distribution in figure 6(b) that does not permit such a distinction. The electron temperature gradient has also been eroded. The electron phase space density decreases by an order of magnitude as we go from  $v_x = 0$  to  $v_x \approx 2v_{t1}$  at  $x \approx 0$  and at  $x \approx 2000$  in figure 6(d) and the thermal spread is thus comparable at both locations. We attribute this temperature equilibration to electrostatic instabilities, which were driven by the electron beam that leaked through the boundary at  $x = 0$ , and also to the electron scattering by the simulation noise. The noise amplitude is significant in the interval  $x > 0$  due to the comparatively low statistical representation of the plasma, in particular that of the hot leaked electrons.

The electron density jumps at both times in figure 6 at the positions, where the protons of plasmas 1 and 2 intersect. The electron distribution for  $S_2$  furthermore shows a spatially uniform distribution in  $450 < x < 550$ , as the protons do. The electrons have thermalized and any remaining free energy would be negligible compared with that of the protons. The

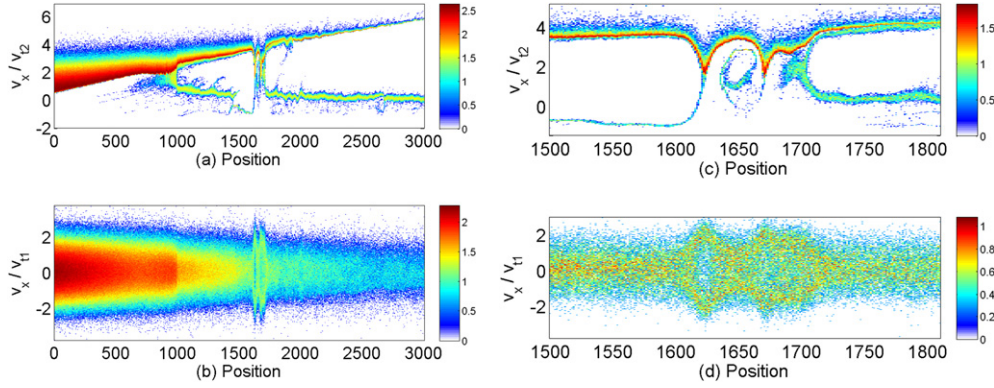


**Figure 7.** The 10-logarithmic phase space density for  $S_3$  in units of CPs: (a) displays the proton distribution and (b) the electron distribution. The shock is located at  $x \approx 900$  and phase space holes develop in the proton (c) and electron (d) distribution at  $1600 < x < 1700$ . A new shock grows at  $x \approx 1700$  in (c). (Colour online.)

electron density merely follows that of the protons to conserve the plasma quasi-neutrality. This electron distribution thus differs from the similarly looking one, which has been computed recently in [21]. There the electrons changed their velocity distribution in response to the energy lost to the protons.

The time  $10t_S$  corresponding to  $S_1$  and the box length  $L_L = 10L_S$  imply that we should see some electrons emanated by the plasma boundary at  $x = L_L/2$  as in figure 5. Only the electrons with  $v < -2.1v_{t1}$  would be fast enough to cross the interval  $0 < x < L_L/2$  occupied by plasma 2 during the time  $10t_S$ . These electrons correspond to the few fast electrons in figure 6(b) with  $x > 0$  and  $v < 0$ . An increased number of fast electrons moving in the negative  $x$ -direction is visible at the snapshot  $S_2$ . The electrons emanated from the plasma boundary at  $x = L_L/2$  now reach the boundary at  $x = 0$  in significant numbers. The diffuse phase space distribution of these electrons implies, however, that they do not carry with them enough free energy that could result in instabilities that drive strong electrostatic fields.

The shock structure and the density jump in the electron distribution has propagated to  $x \approx 900$  for  $S_3$  and the proton beam ahead of the shock has started to thermalize by its interaction with the upstream plasma, as it is evidenced in figure 7. An electron phase space hole doublet and proton phase space structures are visible. These structures have grown out of the phase space oscillation of the proton beams and the electron phase space hole at  $x \approx 1250$  in figure 6(c). The proton distribution in figure 7(c) in  $x \geq 1700$  reveals that a second shock forms, which will thermalize the dense and fast beam of protons that expands out of plasma 1 into plasma 2. The spatially uniform electron distribution outside the interval occupied by the electron phase space holes changes only its thermal spread and density along  $x$  and could be approximated by a Boltzmann distribution. The electrons are not accelerated to high energies neither by the shocks nor by the other phase space structures.

The expansion of the protons of plasma 1 in simulation 2 is captured by movie 3 ([stacks.iop.org/PPCF/52/025001](http://stacks.iop.org/PPCF/52/025001)). The colour scale corresponds to the 10-logarithmic number of CPs. Movie 3 evidences the formation of the shock and of its downstream region and it displays how the proton phase space hole and, subsequently, the secondary shock develop. The mean velocity of the upstream protons is modulated along  $x$ , which is probably a result of the same wave fields that thermalized the electrons.

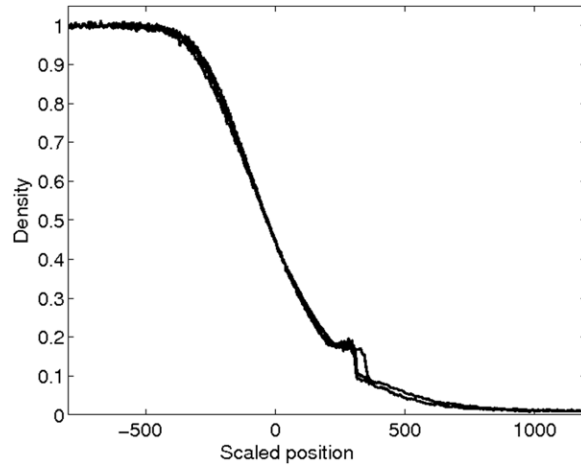


**Figure 8.** The proton densities, normalized to  $n_h$ , as a function of the scaled position  $xt_1/t_j$ , where  $t_j$  corresponds to the snapshot  $S_j$ . The curves match, except within the downstream region of the shock at  $200 < xt_1/t_j < 400$  that is characterized by a constant density. The density doubles by the shock compression at  $xt_1/t_j \approx 350$ .

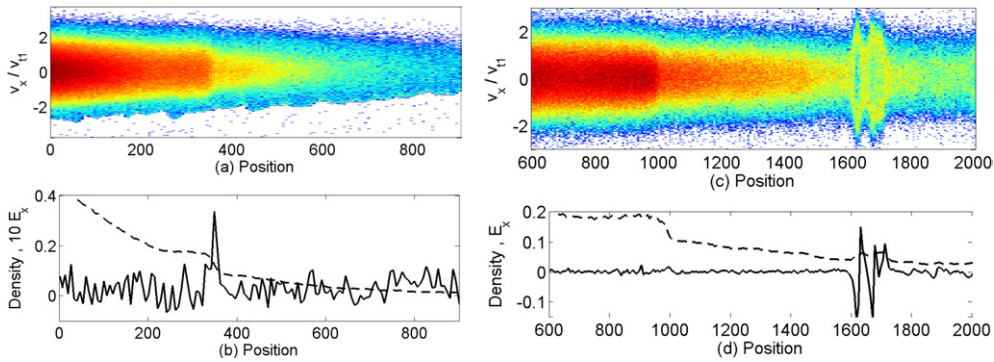


**Figure 9.** The 10-logarithmic electron phase space distributions are shown in (a) for  $S_1$  and (c) for  $S_3$ . The electron density (dashed curves) and the electrostatic field (solid curves) are displayed in (b) for  $S_1$  and in (d) for  $S_3$ . The densities are integrated and the electric fields averaged over 5 grid cells. (Colour online.)

The proton distribution at  $x \approx 0$  changes in time primarily due to the free motion of a proton  $i$  with the speed  $v_{x,i}$ , which is displaced as  $x_i = v_{x,i}t$ . The phase space boundary between plasmas 1 and 2 is thus increasingly sheared. Further acceleration mechanisms are the drag of the protons by the thermally expanding electrons and the shock formation. Figure 8 assesses their relative importance. The plasma density distribution should be invariant if the protons expand freely and if we scale the position  $\propto x/t$ . This is indeed the case and the proton density distributions for  $S_1$ ,  $S_2$  and  $S_3$  match if we use the scaled positions, except at the shock and within its downstream region. The electron densities (not shown) closely follow those of the protons.

Figure 9 compares the electrostatic field with the electron distributions for snapshots  $S_1$  and  $S_3$ . An electric field peak at  $x \approx 400$  coincides with the shock in snapshot  $S_1$ . The peak  $E_x \approx 0.04$  and it confines the electrons to the left of the density jump by accelerating

them into the negative  $x$ -direction. The electric field can be scaled to physical units with  $n_M = 10^{15} \text{ cm}^{-3}$  and  $v_{t1} = 1.325 \times 10^7 \text{ m s}^{-1}$  to give  $\approx 5 \times 10^6 \text{ V m}^{-1}$ . The electric field, which has been measured close to the shock in [8], is  $\leq 2 \times 10^7 \text{ V m}^{-1}$ . The plasma density in the region, where the shock develops in the experiment, may be higher than  $10^{15} \text{ cm}^{-3}$ . The electric field amplitudes associated with the shock are thus comparable. The noise levels in PIC simulations are typically higher than in a physical plasma, explaining the strength of the evenly spread noise in the simulation box, which is not observed to the same extent in the experiment. The electric field at the shock at  $x \approx 10^3$  is at noise levels for  $S_3$ , while the phase space holes at  $x \approx 1700$  give an electric field, which exceeds that sustained by the shock for  $S_1$ .

## 5. Discussion

We have investigated the thermal expansion of a hot dense plasma into a cold tenuous plasma. The thermal pressure of the hot plasma exceeded that of the cold plasma by a factor of  $10^4$ . Our study has been motivated by the laser-plasma experiment in [8], which examined the expansion of a hot and dense plasma into a tenuous ambient medium. Our initial conditions and the 1D geometry are, however, idealized and the simulation results thus cannot be compared quantitatively with the experimental ones. The aim of our work has been to better understand the qualitative effects of the ambient medium on the plasma expansion. We have, for this purpose, compared our results with some of those in the related study in [21], which considered the plasma expansion into a vacuum. There, the electron temperature exceeded that of the protons by a factor of  $10^3$ , while we consider here the same temperature of electrons and protons.

Our results are summarized as follows. An electric field grows almost instantly at the boundary between both plasmas, because the ion expansion of the hot plasma is slower than the electron expansion. The electric field forms irrespective of the ambient medium. It accelerates only the ions, if the plasma expands into a vacuum and it has a cusp in its spatial profile. The acceleration of the electrons of the ambient medium triggers in our simulation the formation of a double layer [22] with a smooth electric field profile. This double layer redistributes the momentum between the individual plasma species [25]. A tenuous hot beam of electrons streams from the hot plasma into the cold plasma, while all the electrons of the cold plasma are dragged into the hot plasma. These beams thermalize through electrostatic two-stream instabilities, which equilibrate the electron temperatures of both plasmas on electron time scales. This rapid thermalization will cancel any significant proton acceleration by hot electrons already at the relatively low density of the ambient medium we have used. Proton acceleration is, however, still possible because a thermal pressure gradient is provided by the density jump. Most electrons merely follow after their thermalization the motion of the protons to conserve the quasi-neutrality of the plasma. They maintain their Maxwellian velocity distribution, which would not be the case for an expansion into a vacuum [21].

The protons at the front of the hot plasma are accelerated by the electric field of the double layer to about 5.5 times the proton thermal speed, while the Maxwellian distribution is represented up to 3–4 times the proton thermal speed. The expansion of the protons from the hot into the cold plasma is dominated by the free streaming of the fastest protons (diffusion). The effects of the ambient medium on the proton expansion are initially negligible. Eventually the interaction of the expanding and the ambient plasma results in the formation of shocks. We have observed one shock at the position, where the protons of both plasmas merge. This shock did not result in the acceleration of electrons or in the modification of their phase space distribution.

The protons of the hot plasma expand farther than the position of this shock and they can interact with the protons of the cold plasma through ion beam instabilities. The interval, in

which the protons of both plasmas co-exist, qualitatively resembles the upstream region of an electrostatic shock [11]. However, the density and the speed of the beam of expanding protons of the hot plasma are both higher than what we expect for a shock-reflected ion beam. We have observed in the simulation the growth of a phase space structure in the upstream proton distribution that gave rise to an electron phase space hole. The proton structure evolved into a second shock ahead of the primary one. The presence of multiple shocks has been observed experimentally [26], although there the second shock was radiation-driven and not beam-driven.

### Acknowledgments

The authors acknowledge the financial support by an EPSRC Science and Innovation award, by the visiting scientist programme of the Queen's University Belfast, by Vetenskapsrådet and by the Deutsche Forschungsgemeinschaft (Forschergruppe FOR1048). The HPC2N computer center has provided the computer time.

### References

- [1] Koopman D W and Tidman D A 1967 *Phys. Rev. Lett.* **18** 533
- [2] Bell A R *et al* 1988 *Phys. Rev. A* **38** 1363
- [3] Remington B A, Arnett D, Drake R P and Takabe H 1999 *Science* **284** 1488
- [4] Woolsey N C *et al* 2001 *Phys. Plasmas* **8** 2439
- [5] Drury L O and Mendonca J T 2000 *Phys. Plasmas* **7** 5148
- [6] Borghesi M *et al* 2002 *Phys. Rev. Lett.* **88** 135002
- [7] Romagnani L *et al* 2005 *Phys. Rev. Lett.* **95** 195001
- [8] Romagnani L *et al* 2008 *Phys. Rev. Lett.* **101** 025004
- [9] Molvig K 1975 *Phys. Rev. Lett.* **35** 1504
- [10] Bret A, Firpo M C and Deutsch C 2005 *Phys. Rev. Lett.* **94** 115002
- [11] Forslund D W and Freidberg J P 1971 *Phys. Rev. Lett.* **27** 1189
- [12] Cheng C Z and Knorr G 1976 *J. Comput. Phys.* **22** 330
- [13] Dawson J M 1983 *Rev. Mod. Phys.* **55** 403
- [14] Eastwood J W 1991 *Comput. Phys. Commun.* **64** 252
- [15] Sack C and Schamel H 1987 *Phys. Rep.* **156** 311
- [16] Sack C, Schamel H and Schmalz R 1986 *Phys. Fluids* **29** 1337
- [17] Manfredi G, Mola S and Feix M R 1993 *Phys. Fluids B* **5** 388
- [18] Dorozhkina D S and Semenov V E 1998 *Phys. Rev. Lett.* **81** 2691
- [19] Mora P 2003 *Phys. Rev. Lett.* **90** 185002
- [20] Mora P and Grismayer T 2009 *Phys. Rev. Lett.* **102** 145001
- [21] Grismayer T, Mora P, Adam J C and Heron A 2008 *Phys. Rev. E* **77** 066407
- [22] Ishiguro S, Kamimura T and Sato T 1985 *Phys. Fluids* **28** 2100
- [23] Smith R A 1982 *Phys. Scr.* **T2A** 238
- [24] Raadu M A and Rasmussen J J 1988 *Astrophys. Space Sci.* **144** 43
- [25] Fruchtman A 2006 *Phys. Rev. Lett.* **96** 065002
- [26] Hansen J F, Edwards M J, Froula D H, Edens A D, Gregori G and Ditmire T 2006 *Phys. Plasmas* **13** 112101
- [27] Dupree T H 1963 *Phys. Fluids* **6** 1714
- [28] Jones M E, Lemons D S, Mason R J, Thomas V A and Winske D 1996 *J. Comput. Phys.* **123** 169
- [29] Sentoku Y, Mima K, Kojima S and Ruhl H 2000 *Phys. Plasmas* **7** 689
- [30] Huba J D 1994 *NRL Plasma Formulary* (Washington: Naval Research Laboratory) p 28
- [31] Weibel E S 1959 *Phys. Rev. Lett.* **2** 83
- [32] Stockem A, Dieckmann M E and Schlickeiser R 2009 *Plasma Phys. Control. Fusion* **51** 075014
- [33] Birdsall C K and Maron N 1980 *J. Comput. Phys.* **36** 1